



Rapid capture and efficient removal of low-concentration SO₂ in simulated flue gas by hypercrosslinked hollow nanotube ionic polymers

Xue-Cong An^a, Zhang-Min Li^a, Yan Zhou^a, Wenshuai Zhu^b, Duan-Jian Tao^{a,*}

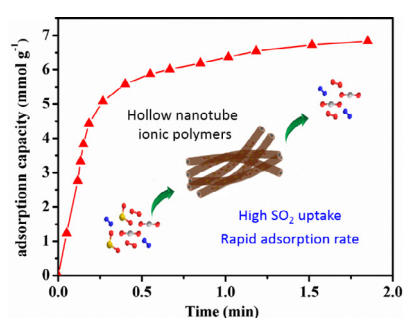
^a College of Chemistry and Chemical Engineering, Jiangxi Normal University, Nanchang 330022 China

^b School of Chemistry and Chemical Engineering, Institute for Energy Research, Jiangsu University, Zhenjiang 212013 China

HIGHLIGHTS

- Novel hypercrosslinked hollow nanotube ionic polymers were prepared.
- A rapid SO₂ adsorption rate was obtained with less than 2 min.
- High SO₂ capacity and outstanding SO₂/N₂ and SO₂/CO₂ selectivity were achieved.
- HNIP-TBMB-1 showed good reversibility in adsorption–desorption cycles.

GRAPHICAL ABSTRACT



ARTICLE INFO

Keywords:

Ionic polymers
Hollow nanotube
Hypercrosslinked ionic polymers
SO₂ capture
Adsorption

ABSTRACT

It is very challenging to design efficient adsorbent materials for SO₂ capture with fast adsorption rate and with high capacity and selectivity, simultaneously. In this work, a kind of hypercrosslinked hollow nanotube ionic polymers (HNIPs) is reported for rapid capture and efficient removal of low-concentration SO₂ in simulated flue gas. The HNIP-TBMB-1 exhibited very high SO₂ capacity (7.2 mmol g⁻¹) and outstanding SO₂/N₂ (3186) and SO₂/CO₂ (91) selectivity at 298 K and 1 bar. Additionally, HNIP-TBMB-1 also showed unprecedented SO₂ adsorption rate and reduced the equilibrium time to 1.75 min, as well as the diffusion time constant correlated by Fick's diffusion model was estimated to be 0.25 min⁻¹. Dynamic breakthrough experiments further demonstrated the excellent performance of HNIP-TBMB-1 in removing 3000 ppm SO₂ in simulated flue gas. In addition, HNIP-TBMB-1 showed good reversibility in adsorption–desorption cycles. The present work demonstrates that designing a HNIP material that has the special architectural feature of hollow nanotubes with inner-channels can be an effective strategy for realizing efficient, selective, and rapid SO₂ capture.

1. Introduction

The emission of sulfur dioxide (SO₂) from flue gas (cat. SO₂ = 500 ~ 3000 ppm) is mainly induced by the excessive combustion of low-grade coal and fuels. It becomes a huge threat to the natural environment and human health [1–3]. Nowadays, a commonly used strategy to handle this problem is absorption in liquid solvents [4–6].

About 90–95% SO₂ from flue gas can be removed by the traditional flue gas desulfurization (FGD) processes using ammonia or wet limestone as the absorbents [7]. However, these FGD processes are energy intensive and not efficient for the removal of trace SO₂ in flue gas. Therefore, the exploration of efficient absorbents/adsorbents for deep desulfurization of flue gas is constantly and highly demanded.

It is well known that a porous material possessing a large surface

* Corresponding author.

E-mail address: djtao@jxnu.edu.cn (D.-J. Tao).

<https://doi.org/10.1016/j.cej.2020.124859>

Received 19 February 2020; Received in revised form 20 March 2020; Accepted 21 March 2020

Available online 24 March 2020

1385-8947/ © 2020 Elsevier B.V. All rights reserved.

area shows great potential in gas storage/separation [8–12]. In the past decades, various porous materials such as porous polymer [13,14], N-doped carbon materials [15], metal–organic frameworks (MOFs) [16,17], and covalent organic frameworks (COFs) [18,19] have widely been reported for highly efficient, selective, and reversible SO₂ capture. For example, Savage et al. [20] demonstrated that a robust MOF material MFM-300(In) showed a high SO₂ capacity of 8.28 mmol g⁻¹ at 298 K and 1.0 bar through the specific multiple supramolecular interactions. Xing et al. [21] reported a series of inorganic anion-pillared MOFs for ultrahigh and selective SO₂ uptake (11.01 mmol g⁻¹ in SIFSIX-1-Cu) through multiple synergistic host–guest and guest–guest interactions. However, it should be noted that adsorption kinetics is a very important property for practical and industrial application. Many porous adsorbents MOFs that afford high surface area (> 300 m²/g) and abundant microporosity could not realize satisfactory adsorption rate of SO₂, resulting in a very long saturation time (≥ 30 min) [22]. More importantly, it is generally accepted that the mesoporosity in porous adsorbents is favorable for mass transfer of gas molecules and would enhance the adsorption rate. For this reason, the design and synthesis of mesoporous materials but with very fast gas uptake rate is a very attractive strategy for efficient and deep removal of SO₂.

Recently, porous ionic polymers (PIPs), as a kind of porous organic polymers (POPs), have been widely investigated in the fields of gas storage, separation, and utilization (etc. CO₂, CH₄, H₂) owing to their specific properties as hypercrosslinked network and strong interaction capacitated by abundant ionic groups [23–25]. However, there has been less attention paid to the utilization of PIPs for efficient and selective SO₂ capture [24]. In this context, it is desirable and worth to design and prepare novel highly crosslinked PIPs for efficient, selective, and fast adsorption of SO₂.

Herein, we prepared a kind of hypercrosslinked mesoporous hollow nanotube ionic polymers (HNIPs) by the two-step process involving the first step of quaternarization and the second step of Friedel–Crafts alkylation (Scheme 1). This kind of novel HNIPs could act as efficient adsorbents for SO₂ capture with both very fast adsorption rate and high capacity simultaneously (7.2 mmol·g⁻¹ within 0.5 ~ 2 min at 298 K and 1 bar). Also, these HNIPs exhibited unprecedented selectivity of SO₂ over other gases, e.g., the adsorption amount ratio of SO₂/N₂ and SO₂/CO₂ were up to 3186 and 91 at 298 K and 1 bar, respectively. Furthermore, the excellent actual SO₂ separation performance was evaluated via column breakthrough experiments with a simulated flue gas composition.

2. Experimental

2.1. Materials

4,4'-Bipyridine (4,4'-bpy, 98%), 1,3,5-tris(1,3,5-bromomethyl)benzene (TBMB, 98%), 1,4-dichloroxylylene (DCX, 98%), 1,2-dichloroethane (99.5%), and anhydrous iron chloride (FeCl₃, CP) were provided by

Shanghai Macklin Biochemical Co., Ltd. Carbon dioxide (CO₂, 99.99 v/v%), sulfur dioxide (SO₂, 99.99 v/v%), nitrogen (N₂, 99.99 v/v%) and helium (He, 99.99 v/v%) were purchased from Jiangxi Huate Special Gas Co., Ltd. All chemicals and other reagents were used without any further purification.

2.2. Preparation of HNIPs

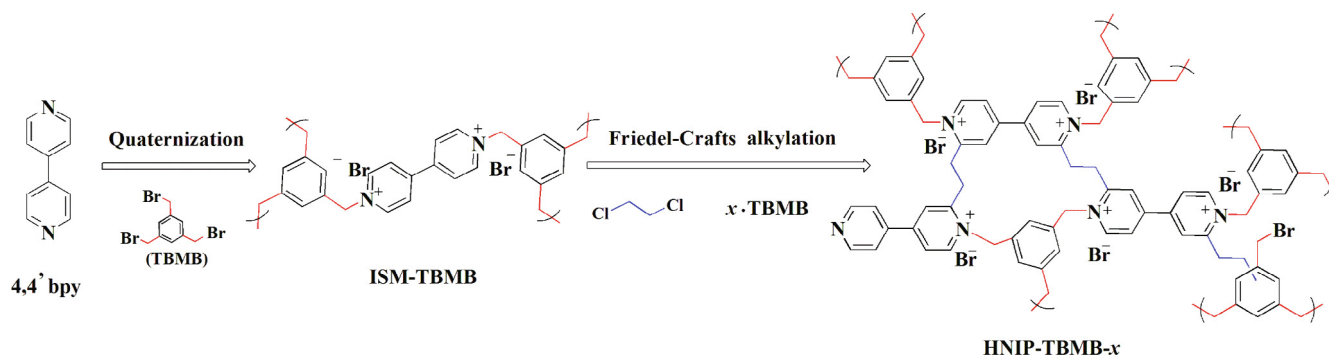
Scheme 1 illustrates the preparation of HNIP-TBMB-*x* (*x* = the mass ratio of TBMB to ISM-TBMB) via a two-step procedure consist of quaternarization and Friedel–Crafts alkylation (Scheme 1). The schematic diagram for synthesis of HNIP-DCX-*y* (*y* = the mass ratio of DCX to ISM-DCX) is also shown in Scheme S1 in Supplementary data.

Synthesis of precursor ionic salt monomer (ISM): In a typical run, TBMB (1.46 g, 4 mmol) in CH₃CN (15 mL) was slowly added to a solution of 4,4'-bpy (0.30 g, 2 mmol) in CH₃CN (15 mL) within 1 h. The mixture was stirred and refluxed at 353 K for 24 h. After reaction, the precipitate was filtered from the mixture and washed with CH₂Cl₂ (3 × 15 mL). Then a yellow powder was obtained and dried in high vacuum for 24 h at 353 K. The as-prepared precursor was denoted as ISM-TBMB. Similarly, another precursor ISM-DCX was prepared in according to the synthesis procedure of ISM-TBMB with the replacement of DCX to TBMB.

Synthesis of hollow nanotube ionic polymers (HNIPs): In a typical run, ISM-TBMB (0.30 g), TBMB (0.30 g), and FeCl₃ (0.3 mmol, 0.55 g) were dissolved in 1,2-dichloroethane (30 mL). Then, the mixture was stirred at 353 K for 24 h under N₂ atmosphere. After reaction, the brown precipitate was followed by filtration and washed with methanol (3 × 25 mL), deionized water (3 × 25 mL), and CH₂Cl₂ (3 × 25 mL), respectively. In order to remove possible traces of FeCl₃, the brown precipitate was further purified by Soxhlet extraction with methanol for 24 h. Thus, a brown powdery solid HNIP-TBMB-1 was obtained with and dried in high vacuum for 24 h at 353 K. Likewise, HNIP-TBMB-2 was prepared as the same synthesis procedure of HNIP-TBMB-1, except with the mass ratio of TBMB to ISM-TBMB by 2:1. Using the precursor ISM-DCX, HNIP-DCX-1 was also prepared with the mass ratio of DCX to ISM-DCX by 1:1.

2.3. Characterizations

The morphology and sizes of samples were characterized using both field emission scanning electron microscope (SEM, HITACHI SU8020) with a cold field-emission instrument and transmission electron microscopy (TEM, JEOL JEM-2100). The surface chemical composition was determined by X-ray photoelectron spectroscopy (XPS, Thermo Scientific ESCALAB 250Xi, Al Kα radiation source). Fourier transform infrared (FTIR) spectra were recorded on a Nicolet 6700 spectrometer. Thermogravimetric analysis (TGA) was carried out on a PerkinElmer Diamond TG/DTA apparatus from room temperature to 1073 K at a constant heating rate of 10 K min⁻¹ under flowing nitrogen.



Scheme 1. The two-step synthesis procedure of HNIP-TBMB-*x*.

2.4. Adsorption measurements

The measurement of SO₂ adsorption was recorded on a dual chamber volumetric adsorption apparatus (Fig. S1, Supplementary data), according to our previous work on CO₂ and CO adsorption [26–29]. After the completion of SO₂ uptake, the SO₂-loaded HNIP-TBMB-1 sample was heated at 353 K for 0.5 h under a vacuum of 0.01 bar to release the captured SO₂. Then the recycled HNIP-TBMB-1 was reused for the next SO₂ adsorption run. The single-component adsorption isotherms of CO₂ and N₂ at 298 K were measured in a Micromeritics TriStar II 3020 adsorption apparatus. The samples were degassed at 373 K and vacuumed for 12 h to remove residual moisture and other trapped gases before N₂ and CO₂ adsorption analysis. The specific Brunauer – Emmett – Teller (BET) surface area was calculated based on the N₂ adsorption isotherms at 77 K.

3. Results and discussion

3.1. Characterization of HNIPs

Two kinds of hypercrosslinked mesoporous ionic polymers HNIP-TBMB and HNIP-DCX were successfully prepared (Scheme 1, Scheme S1) and they are insoluble in several organic solvents such as methanol, ethyl acetate, diethyl ether, tetrahydrofuran, and dimethyl sulfoxide. Fig. 1 shows the FTIR spectra of ISM-TBMB, HNIP-TBMB-1, and HNIP-TBMB-2. It is showed that these three samples exhibited typical stretching vibrations peaks of the skeletal benzene ring at 1450, 1500, and 1600 cm⁻¹. The characteristic peak at 1635 cm⁻¹ were also observed in these three samples, which ascribes to the C = N stretching of quaternized pyridine ring. This indicates that the quaternarization reaction was successfully performed in the synthesis of ISM-TBMB, HNIP-TBMB-1, and HNIP-TBMB-2. Moreover, it should be noted that 1,2-dichloroethane could act as a direct external cross-linker to form the hyper-cross-linking polymer network through the Friedel-Crafts reaction (Scheme 1) [30,31]. Compared with the FTIR spectra of ISM-TBMB, one new characteristic peak was observed at 1384 cm⁻¹ for both HNIP-TBMB-1 and HNIP-TBMB-2, which assigns to the C – H bending vibration of –CH₂ group originated from 1,2-dichloroethane.

Fig. 2 demonstrates the morphologies of HNIP-TBMB-1 and HNIP-TBMB-2, respectively. SEM and TEM images indicate that all the two HNIP-TBMB samples had a uniform 1D tubular morphology. HNIP-TBMB-1 had an external diameter of around 80 nm and inner diameter of 30 ~ 50 nm, as well as HNIP-TBMB-2 had an average outer diameter of 90 nm and inner diameter of 50 ~ 70 nm, respectively. Moreover,

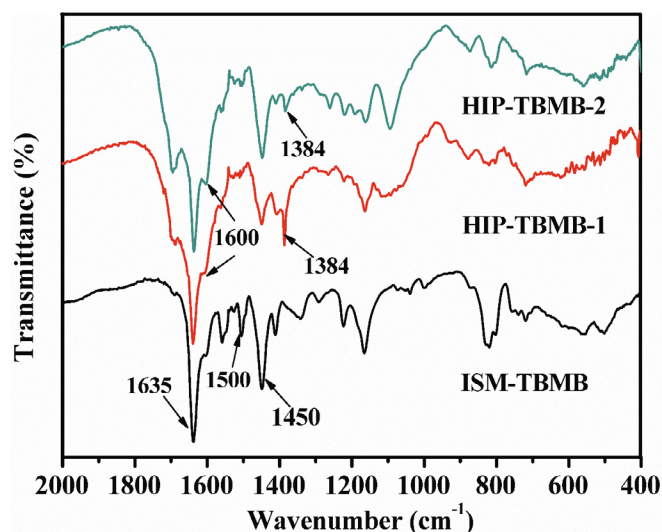


Fig. 1. FTIR spectra of ISM-TBMB and HNIP-TBMB.

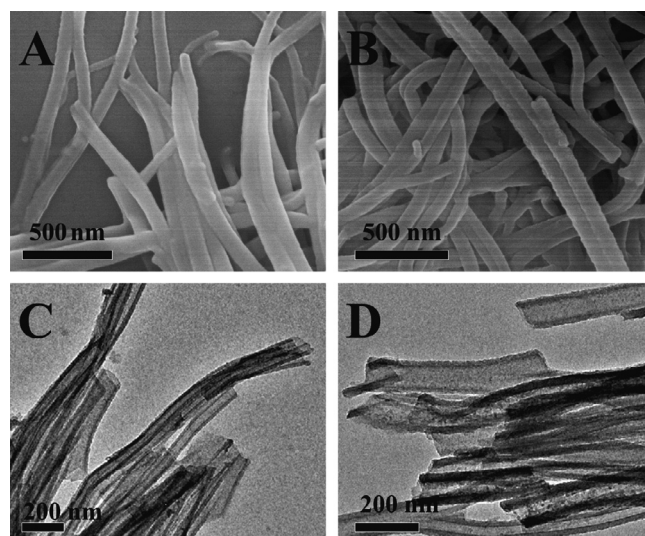


Fig. 2. (A) SEM and (C) TEM images of HNIP-TBMB-1. (B) SEM and (D) TEM images of HNIP-TBMB-2.

TEM line scanning profile of carbon element showed that the carbon signal in the core is much weaker than that on the wall (Fig. S3, Supplementary data), which obviously demonstrates that HNIP-TBMB-1 is a nanotube with a hollow structure instead of a nanofiber [32].

Surface area and pore structure of the obtained HNIP-TBMB were measured by N₂ adsorption–desorption analysis (Fig. 3). The isotherms of ISM-TBMB sample exhibited very low N₂ adsorption capacity, indicating the nonporosity of ISM-TBMB. All the HNIP-TBMB samples displayed a type-IV isotherm with an obvious H3 hysteresis loop, which indicates the pores were mainly slit-shaped. HNIP-TBMB-1 sample had a very low surface area of 45 m²/g, and the N₂ uptake mainly occurred at 0.9 ~ 1.0P/P₀, indicating the presence of a little mesopores and abundant macroporous structures (Fig. S4, Supplementary data). For comparison, HNIP-TBMB-2 and HNIP-DCX-1 exhibited the large surface area of 155 and 207 m²/g, respectively (Table 1). These two isotherms all displayed a H3 hysteresis loop at relative pressure from 0.2 to 1.0P/P₀, and the steep uptake of N₂ was observed at relative pressure of 0.9 ~ 1.0 (Fig. 3, Fig. S5, Supplementary data). Also, the pore size distribution curves manifested that HNIP-TBMB-2 and HNIP-DCX-1 had rich hierarchical meso-macroporous structure (Figs. S6, S7, Supplementary data). Thus, it is believed that a large mass ratio of TBMB to ISM-TBMB is beneficial to the degree of crosslinking reaction

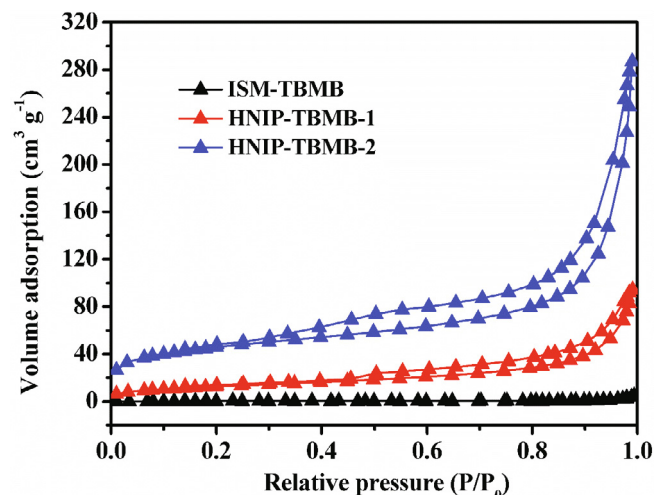


Fig. 3. N₂ adsorption/desorption isotherms of ISM-TBMB and HNIP-TBMB.

Table 1
Comparison of separation performance of HNIP-TBMB with other adsorbents at 298 K and 1 bar.

Samples	S_{BET} ($\text{m}^2 \text{g}^{-1}$)	SO_2 (mmol g^{-1})		Uptake time (min)	SO_2/CO_2 (10:90)	SO_2/N_2 (10:90)	Ref
		0.1 bar	1.0 bar				
HNIP-TBMB-1	45	3.54	7.20	1.75	91	3186	this work
HNIP-TBMB-2	155	3.39	7.07	2	50	3051	this work
HNIP-DCX-1	207	1.57	4.80	2	23	336	this work
PI-COF-m60	93	–	4.74	20	–	–	[18]
NPC-1-900	1656	–	1.85	30	–	–	[36]
SIFSIX-3-Zn	250	1.89	2.10	–	276	507	[21]
ELM-12	706	1.95	2.73	–	30	4064	[37]
MFM-300(In)	1071	7.20	8.28	–	50	2700	[20]
SIFSIX-1-Cu	1178	8.70	11.00	–	71	3146	[21]
MFM-601	3644	5.00	12.30	–	32	255	[17]

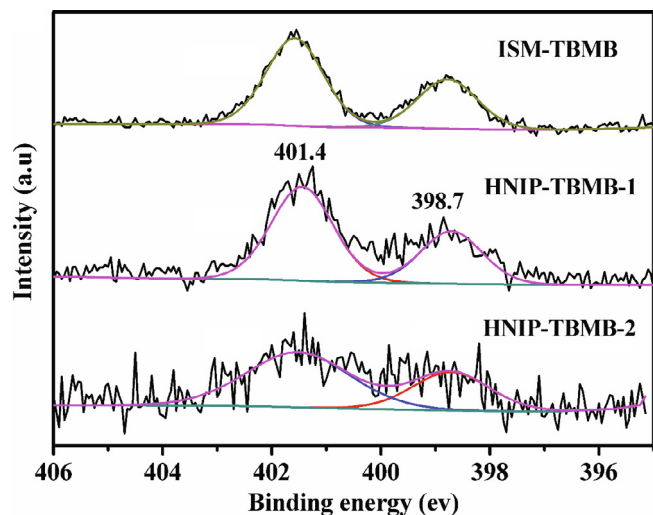


Fig. 4. XPS N 1s spectra of ISM-TBMB and HNIP-TBMB.

and results to the larger specific BET surface areas [33].

To gain an insight into the detailed surface elemental compositions of the ISM-TBMB and HNIP-TBMB samples, XPS measurements were performed and the results are shown in Fig. 4. The N 1s XPS spectra were deconvoluted into two distinct peaks. The peaks at the binding energies of 398.7 eV and 401.4 eV can be assigned to pyridinic N and quaternary N, respectively [34,35], respectively. This result again confirms that the quaternization of 4,4'-bpy had successfully proceed for synthesis of ISMB and HNIP-TBMB. In addition, the TGA analysis further showed that the HNIP-TBMB materials as well as the precursor ISMB have good thermal stability, in which all the decomposition temperatures are higher than 500 K (Fig. S8, Supplementary data).

3.2. SO_2 adsorption and separation performance

The adsorption isotherms of SO_2 on HNIP-TBMB-1, HNIP-TBMB-2, and HNIP-DCX-1 were measured to evaluate their SO_2 capture ability. As shown in Fig. 5, HNIP-TBMB-1 and HNIP-TBMB-2 exhibited good SO_2 adsorption capacity with the saturation value of 7.20 and 7.03 mg g^{-1} at 298 K and 1 bar, respectively. However, HNIP-DCX-1 exhibited SO_2 adsorption capacity of 4.80 mg g^{-1} at 298 K and 1 bar (Fig. S9, Supplementary data). It is seen from Table 1 that the capability of HNIP-TBMB-1 and HNIP-TBMB-2 are superior to many other porous materials, such as PI-COF-m60 (4.74 mmol g^{-1}) [18], NPC-1-900 (1.85 mmol g^{-1}) [36], ELM-12 (2.73 mmol g^{-1}) [37], and SIFSIX-3-Zn (2.10 mmol g^{-1}) [21] under the same condition. Moreover, in the SO_2 partial pressure of 0.1 bar, HNIP-TBMB-1 and HNIP-TBMB-2 also reached the SO_2 uptake of 3.54 and 3.39 mmol g^{-1} at 298 K, respectively, which accounts for ~50% of the saturation adsorption capacity at 1.0 bar and 298 K. This suggests that HNIP-TBMB-1 and HNIP-TBMB-

2 has great potential in removing low-concentration SO_2 .

Since N_2 and CO_2 usually exist along with SO_2 in most flue gas, a high selectivity is necessary for selective capture of SO_2 in a FGD process. Thus, adsorption isotherms of CO_2 and N_2 on HNIP-TBMB-1, HNIP-TBMB-2, and HNIP-DCX-1 were further determined at 298 K to evaluate the separation selectivity. It is expected that HNIP-TBMB-1 had very less adsorbability on N_2 and CO_2 , owing to its very low specific surface area. For comparison, HNIP-TBMB-2 and HNIP-DCX-1 had large BET surface areas and exhibited relatively high N_2 and CO_2 adsorption capacities (Table 1, Fig. 5A, Fig. 5B, Fig. S9, Supplementary data). Then, IAST selectivity of SO_2/CO_2 and SO_2/N_2 for the HNIP-TBMB-1 and HNIP-TBMB-2 were calculated as a function of varying SO_2 composition (Fig. 5C, Fig. 5D). It is demonstrated that HNIP-TBMB-1 showed the excellent SO_2/CO_2 selectivity (91) for SO_2/CO_2 (10/90, v/v) mixture at 298 K and 1 bar, which is much higher than HNIP-TBMB-2, HNIP-DCX-1, and many reported MOFs materials such as ELM-12 [37], MFM-300(In) [20], SIFSIX-1-Cu [21], and MFM-601 [17] (Table 1). Also, HNIP-TBMB-1 exhibited outstanding SO_2/N_2 selectivities (650–3186) over a wide range of SO_2 molar fraction in gas phase (0.1–0.9). These findings show that the special architectural feature of HNIP-TBMB-1 results to the low BET surface area and thus leads to a very few amount of N_2 and CO_2 adsorption on the hollow nanotubes. On the other hand, the pyridinic-N sites in HNIP-TBMB-1 affords considerable Lewis basicity [36] and is favor for enhanced SO_2 uptake, which is significantly larger than the capability of HNIP-DCX-1. As a result, HNIP-TBMB-1 exhibited the larger SO_2 capacities but a lower N_2 and CO_2 uptake, resulting in excellent SO_2/N_2 and SO_2/CO_2 separation selectivity.

3.3. SO_2 adsorption rate and diffusion model

Adsorption kinetics is another important property for practical desulfurization application. Fig. 6 illustrates the SO_2 adsorption rate on HNIPs at 298 K and 1 bar. Impressively, all of these materials exhibited very satisfactory SO_2 adsorption rate. For example, HNIP-TBMB-1 and HNIP-DCX-1 captured ~80% of saturated SO_2 uptake at 298 K and 1 bar within less than 0.5 min, and they could reach equilibrium within 2 min. The unprecedented SO_2 adsorption rate is much faster than most of available materials including zeolites, organic polymers, pyrolyzed carbons, and MOFs [18,36,38]. The present of HNIPs with mesopore-macropore inner diameters can significantly reduce the mass transfer of gas molecules and thus facilitate the diffusion and adsorption of SO_2 in the channels of hollow nanotubes.

Furthermore, the Fick's diffusion model [39,40] is employed to correlate and fit the data for SO_2 adsorption on HNIP-TBMB-1 using the following equation:

$$1 - \frac{m_t}{m_{\text{max}}} = \frac{6}{\pi^2} \exp\left(-\pi^2 \frac{D_c t}{r_c^2}\right)$$

where m_t (mmol g^{-1}) is the amount of SO_2 adsorption at time t , m_{max} (mmol g^{-1}) is the saturated adsorption capacity, and m_t/m_{max}

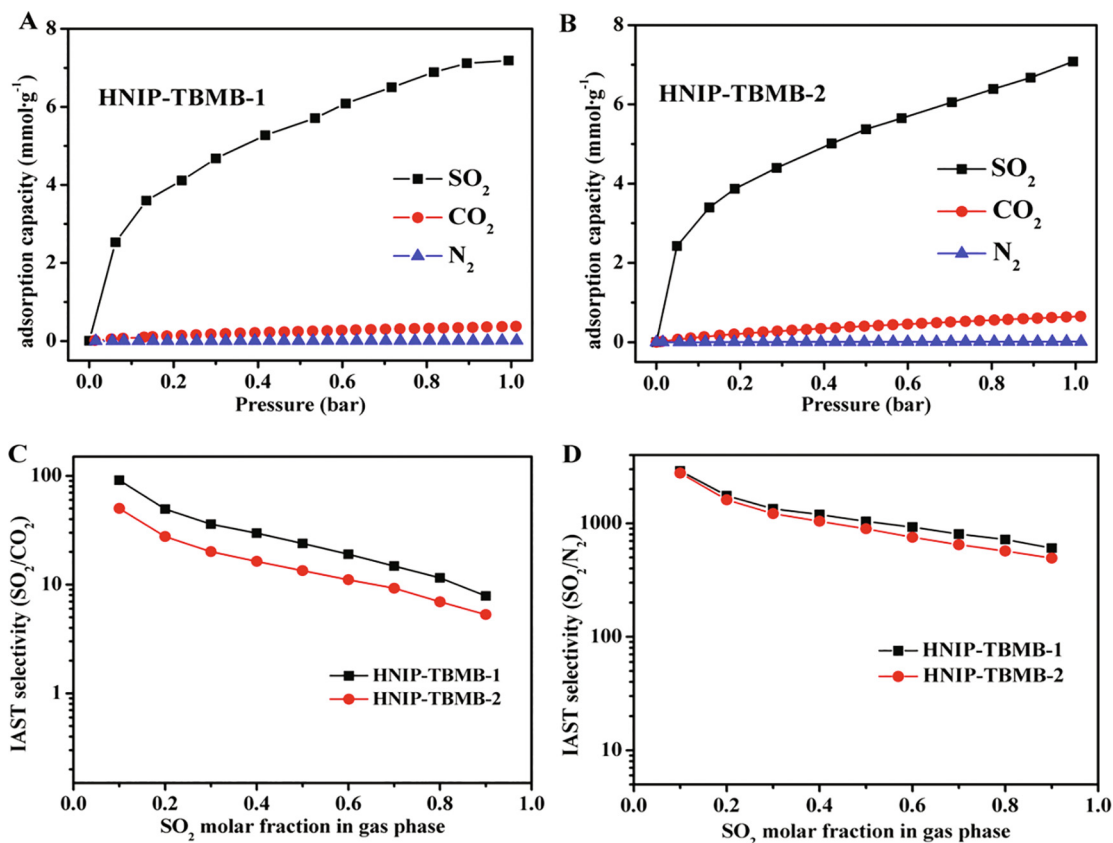


Fig. 5. SO₂, CO₂, and N₂ adsorption isotherms for A) HNIP-TBMB-1 and B) HNIP-TBMB-2 at 298 K and 1 bar. The IAST selectivity of C) SO₂/CO₂ and D) SO₂/N₂ mixtures with varying SO₂ molar fractions in gas phase at 1 bar.

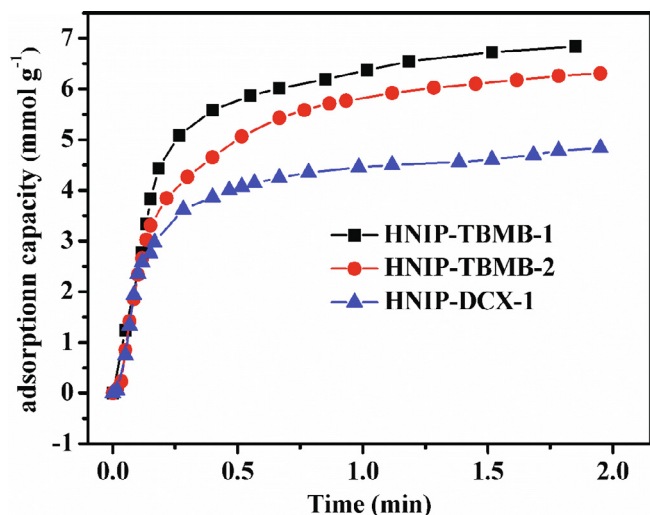


Fig. 6. SO₂ adsorption rate for HNIP-TBMB and HNIP-DCX at 298 K and 1 bar.

represents the fractional SO₂ uptake. The ratio D_c/r_c^2 (min⁻¹) is well known as the diffusion time constant, and it can be estimated and regressed using the data points with fractional SO₂ uptake larger than 70%. It is seen from Fig. 7 that the correlation coefficient R^2 was above 0.95, as well as the Fick's diffusion model had a good fitting for SO₂ adsorption kinetics. Then the SO₂ diffusion time constant for HNIP-TBMB-1 was obtained to be 0.25 min⁻¹, which is much higher than that for biomass derived carbon reported previously [40]. The small value of D_c/r_c^2 means high SO₂ diffusion rate during the adsorption process, which can greatly shorten the adsorption cycle time in FGD applications.

3.4. Dynamic breakthrough performance

To evaluate the actual SO₂/CO₂ and SO₂/N₂ separation performance of HNIPs, dynamic experimental breakthrough tests were carried out with simulated flue gas compositions containing 3000 ppm SO₂ with a flow rate of 10 mL min⁻¹ at 298 K and 1 bar. As shown in Fig. 8, all gases except SO₂ rapidly eluted within 20 min g⁻¹, and highly efficient elimination of SO₂ was achieved with a breakthrough time interval of 430 and 420 min g⁻¹, respectively. This finding demonstrates that HNIP-TBMB-1 and HNIP-TBMB-2 retained the excellent SO₂ separation ability even with the co-existence of N₂, O₂, and CO₂, making a good agreement with the results of adsorption isotherms and IAST calculations. Furthermore, the comparison results of breakthrough tests of HNIP-TBMB with the other adsorbents from the reported literatures also confirmed the excellent performance of HNIP-TBMB-1 (Table S1, Supplementary data). Therefore, HNIPs are considered to have the great potential for practical desulfurization applications.

3.5. Recycling test of HNIP-TBMB-1

The reusability of HNIP-TBMB-1 for SO₂ capture is essential for future practical applications. First, FTIR spectroscopy was performed to assess the reversible SO₂ capture. As seen from Fig. 9A, compared with the IR spectra of the fresh HNIP-TBMB-1, two new characteristic peaks were observed at 1326 and 1034 cm⁻¹ after SO₂ adsorption, which can be assigned to asymmetric S = O stretching vibration and $\pi \cdots S$ interaction between SO₂ and the phenyl group in HNIP-TBMB-1, respectively [41–43]. This suggests that physical adsorption plays a leading role in the adsorption of SO₂ on HNIP-TBMB-1, and it is easy to release the captured SO₂ at 353 K under a vacuum of 0.01 bar. Moreover, there is no obvious change in the characteristic peaks of FTIR spectra between the fresh and reused 12th HNIP-TBMB-1. The high available

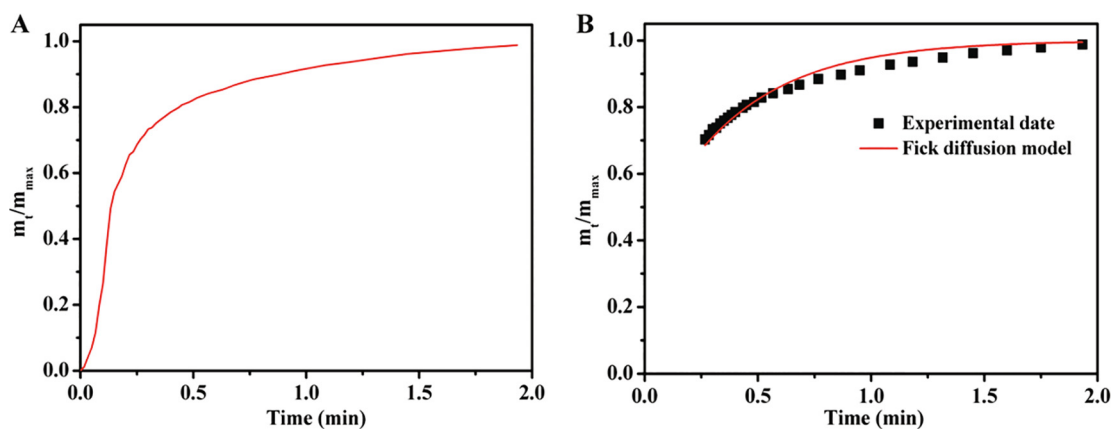


Fig. 7. (A) Adsorption kinetic of SO_2 at 298 K for HNIP-TBMB-1 and (B) Fick's diffusion model on experimental SO_2 uptake of HNIP-TBMB-1.

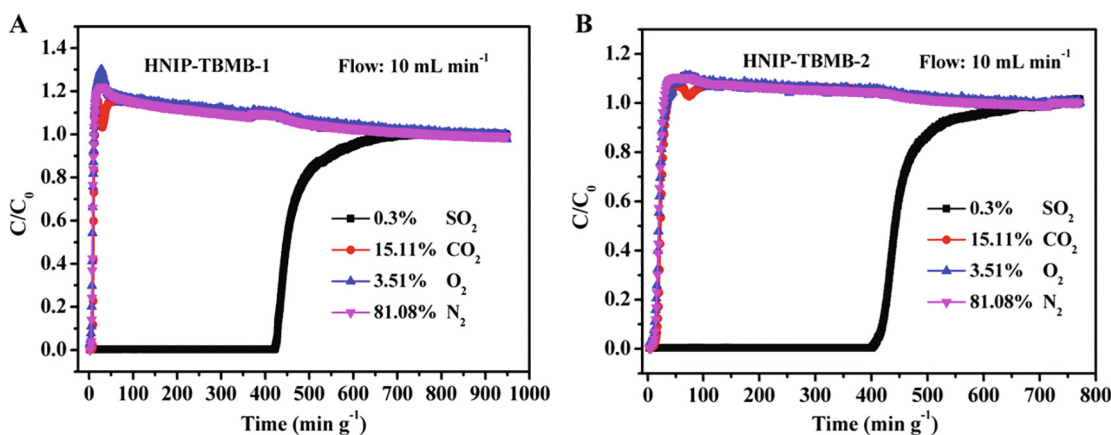


Fig. 8. Experimental column breakthrough curves of A) HNIP-TBMB-1 and B) HNIP-TBMB-2 for simulated flue gas compositions.

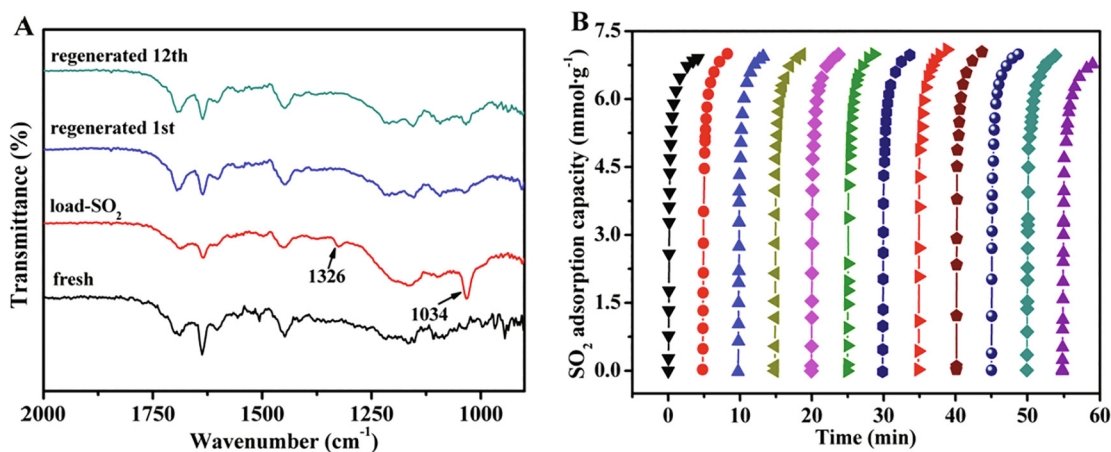


Fig. 9. A) FTIR spectra of fresh, SO_2 -loaded, 1st regenerated, and 12th regenerated HNIP-TBMB-1. B) Recycle performance of HNIP-TBMB-1 for SO_2 adsorption.

adsorption capacity was also well maintained during the twelve cycles (Fig. 9B). All these results demonstrate that the HNIP-TBMB-1 has good stability and reusability for reversible SO_2 capture.

4. Conclusions

In summary, a kind of hypercrosslinked hollow nanotube ionic polymers was prepared and employed for efficient, selective, and rapid SO_2 capture. Owing to the special architectural feature of uniform hollow nanotubes, the highly crosslinked HNIP-TBMB-1 exhibited very high SO_2 capacity (7.2 mmol g^{-1}) and outstanding SO_2/N_2 (3186) and

SO_2/CO_2 (91) selectivity. Notably, HNIP-TBMB-1 also showed unprecedented SO_2 adsorption rate, while the equilibrium time was less than 2 min and the diffusion time constant was estimated to be 0.25 min^{-1} . The breakthrough experiments further demonstrated the excellent performance of HNIP-TBMB-1 in the highly efficient elimination of 3000 ppm SO_2 in simulated flue gas. In addition, HNIP-TBMB-1 showed good reversibility and no obvious decrease in SO_2 capacity was observed during 12 cycles. Therefore, rapid capture and efficient removal of low-concentration SO_2 endows hollow nanotube ionic polymers with good potential for practical desulfurization processes.

Declaration of Competing Interest

The authors declare that they have no known competing financial interests or personal relationships that could have appeared to influence the work reported in this paper.

Acknowledgments

This work was supported by the National Natural Science Foundations of China (Nos. 21566011, 31570560), the Natural Science Foundations of Jiangxi Province (No. 20192ACBL20025), and the Science & Technology Programs of Jiangxi Province Department of Education (No. GJJ160272) for financial support. We also thank Dr. Jun Wang from Nanchang University for column breakthrough tests.

Appendix A. Supplementary data

Supplementary data to this article can be found online at <https://doi.org/10.1016/j.cej.2020.124859>.

Appendix B. Supplementary data

Supplementary data to this article can be found online at <https://doi.org/10.1016/j.cej.2020.124859>.

References

- X. Li, L. Zhang, Y. Zheng, C. Zheng, SO₂ absorption performance enhancement by ionic liquid supported on mesoporous molecular sieve, *Energy & Fuels* 29 (2015) 942–953, <https://doi.org/10.1021/ef5022285>.
- M.H.H.v. Dam, A.S. Lamine, D. Roizard, P. Lochon, C. Roizard, Selective sulfur dioxide removal using organic solvents, *Ind. Eng. Chem. Res.* 36 (1997) 4628–4637, <https://doi.org/10.1021/ie970111f>.
- R. Tailor, A. Ahmadalinezhad, A. Sayari, Selective removal of SO₂ over tertiary amine-containing materials, *Chem. Eng. J.* 240 (2014) 462–468, <https://doi.org/10.1016/j.cej.2013.11.002>.
- K. Zhang, S. Ren, X. Yang, Y. Hou, W. Wu, Y. Bao, Efficient absorption of low-concentration SO₂ in simulated flue gas by functional deep eutectic solvents based on imidazole and its derivatives, *Chem. Eng. J.* 327 (2017) 128–134, <https://doi.org/10.1016/j.cej.2017.06.081>.
- Y. Shang, H. Li, S. Zhang, H. Xu, Z. Wang, L. Zhang, J. Zhang, Guanidinium-based ionic liquids for sulfur dioxide sorption, *Chem. Eng. J.* 175 (2011) 324–329, <https://doi.org/10.1016/j.cej.2011.09.114>.
- R.K. Srivastava, W. Jozewicz, C. Singer, SO₂ scrubbing technologies: A review, *Environ. Prog.* 20 (2001) 219–227, <https://doi.org/10.1002/ep.670200410>.
- R. Tailor, A. Sayari, Grafted propyldiethanolamine for selective removal of SO₂ in the presence of CO₂, *Chem. Eng. J.* 289 (2016) 142–149, <https://doi.org/10.1016/j.cej.2015.12.084>.
- G. Severa, K. Bethune, R. Rocheleau, S. Higgins, SO₂ sorption by activated carbon supported ionic liquids under simulated atmospheric conditions, *Chem. Eng. J.* 265 (2015) 249–258, <https://doi.org/10.1016/j.cej.2014.12.051>.
- H. Peng, J. Zhang, J. Zhang, F. Zhong, P. Wu, K. Huang, J. Fan, F. Liu, Chitosan-derived mesoporous carbon with ultrahigh pore volume for amine impregnation and highly efficient CO₂ capture, *Chem. Eng. J.* 359 (2019) 1159–1165, <https://doi.org/10.1016/j.cej.2018.11.064>.
- J.H. Zhu, Q. Chen, Z.Y. Sui, L. Pan, J. Yu, B.H. Han, Preparation and adsorption performance of cross-linked porous polycarbazoles, *J. Mater. Chem. A* 2 (2014) 16181–16189, <https://doi.org/10.1039/C4TA01537A>.
- G. Liu, Y. Wang, C. Shen, Z. Ju, D. Yuan, A facile synthesis of microporous organic polymers for efficient gas storage and separation, *J. Mater. Chem.* 3 (2015) 3051–3058, <https://doi.org/10.1039/C4TA05349D>.
- C.J. Yoo, P. Narayana, C.W. Jones, Self-supported branched poly(ethyleneimine) materials for CO₂ adsorption from simulated flue gas, *J. Mater. Chem. A* 7 (2019) 19513–19521, <https://doi.org/10.1039/C9TA04662C>.
- Y. Fu, Z. Wang, S. Li, X. He, C. Pan, J. Yan, G. Yu, Functionalized covalent triazine frameworks for effective CO₂ and SO₂ removal, *ACS Appl. Mater. Interfaces* 10 (2018) 36002–36009, <https://doi.org/10.1021/acsami.8b13417>.
- X. Jiang, Y. Liu, J. Liu, X. Fu, Y. Luo, Y. Lyu, Hypercrosslinked conjugated microporous polymers for carbon capture and energy storage, *New J. Chem.* 41 (2017) 3915–3919, <https://doi.org/10.1039/C7NJ00105C>.
- J. Zhang, J. Zhang, M. Li, Z. Wu, S. Dai, K. Huang, Solvent-free and one-pot synthesis of ultramicroporous carbons with ultrahigh nitrogen contents for sulfur dioxide capture, *Chem. Eng. J.* (2019), <https://doi.org/10.1016/j.cej.2019.123579>.
- S. Glomb, D. Woschko, G. Makhloufi, C. Janiak, Metal-organic frameworks with internal urea-functionalized dicarboxylate linkers for SO₂ and NH₃ adsorption, *ACS Appl. Mater. Interfaces* 9 (2017) 37419–37434, <https://doi.org/10.1021/acsami.7b10884>.
- J.H. Carter, X. Han, F.Y. Moreau, I. da Silva, A. Nevin, H.G.W. Godfrey, C.C. Tang, S. Yang, M. Schroder, Exceptional adsorption and binding of sulfur dioxide in a robust zirconium-based metal-organic framework, *J. Am. Chem. Soc.* 140 (2018) 15564–15567, <https://doi.org/10.1021/jacs.8b08433>.
- G.Y. Lee, J. Lee, H.T. Vo, S. Kim, H. Lee, T. Park, Amine-functionalized covalent organic framework for efficient SO₂ capture with high reversibility, *Sci. Rep.* 7 (2017) 557, <https://doi.org/10.1038/s41598-017-00738-z>.
- J. Wang, J. Wang, W. Zhuang, X. Shi, X. Du, Properties of metal-doped covalent organic frameworks and their interactions with sulfur dioxide, *J. Chem.* 1 (8) (2018) 2018, <https://doi.org/10.1155/2018/9321347>.
- M. Savage, Y. Cheng, T.L. Easun, J.E. Eyley, S.P. Argent, M.R. Warren, W. Lewis, C. Murray, C.C. Tang, M.D. Frogley, G. Cinque, J. Sun, S. Rudic, R.T. Murden, M.J. Benham, A.N. Fitch, A.J. Blake, A.J. Ramirez-Cuesta, S. Yang, M. Schroder, Selective adsorption of sulfur dioxide in a robust metal-organic framework material, *Adv. Mater.* 28 (2016) 8705–8711, <https://doi.org/10.1002/adma.201602338>.
- X. Cui, Q. Yang, L. Yang, R. Krishna, Z. Zhang, Z. Bao, H. Wu, Q. Ren, W. Zhou, B. Chen, H. Xing, Ultrahigh and selective SO₂ uptake in inorganic anion-pillared hybrid porous materials *Adv. Mater.* 29 (2017), <https://doi.org/10.1002/adma.201606929>.
- L.M. Rodriguez-Albelo, E. Lopez-Maya, S. Hamad, A.R. Ruiz-Salvador, S. Calero, J.A. Navarro, Selective sulfur dioxide adsorption on crystal defect sites on an isotropic metal organic framework series, *Nat. Commun.* 8 (2017) 14457, <https://doi.org/10.1038/ncomms14457>.
- S.C. Qi, G.X. Yu, D.M. Xue, X. Liu, X.Q. Liu, L.B. Sun, Rigid supramolecular structures based on flexible covalent bonds: A fabrication mechanism of porous organic polymers and their CO₂ capture properties, *Chem Eng. J.* 385 (2020) 123978, <https://doi.org/10.1016/j.cej.2019.123978>.
- D. Xu, J. Guo, F. Yan, Porous ionic polymers: Design, synthesis, and applications *Prog. Polym. Sci.* 79 121 (143) (2018), <https://doi.org/10.1016/j.progpolymsci.2017.11.005>.
- J. Li, D. Jia, Z. Guo, Y. Liu, Y. Lyu, Y. Zhou, J. Wang, Imidazolium based porous hypercrosslinked ionic polymers for efficient CO₂ capture and fixation with epoxides, *Green Chem.* 2675 (2686) (19 2017), <https://doi.org/10.1039/C7GC00105C>.
- F.F. Chen, K. Huang, Y. Zhou, Z.Q. Tian, X. Zhu, D.J. Tao, D.E. Jiang, S. Dai, Multimolar absorption of CO₂ by the activation of carboxylate groups in amino acid ionic liquids *Angew. Chem. Int. Ed.* 55 (2016) 7166–7170, <https://doi.org/10.1002/anie.201602919>.
- D.J. Tao, F.F. Chen, Z.Q. Tian, K. Huang, S.M. Mahurin, D.E. Jiang, S. Dai, Highly efficient carbon monoxide capture by carbanion-functionalized ionic liquids through C-site interactions *Angew. Chem. Int. Ed.* 56 (2017) 6843–6847, <https://doi.org/10.1002/ange.201701919>.
- F.F. Chen, K. Huang, J.-P. Fan, D.-J. Tao, Chemical solvent in chemical solvent: a class of hybrid materials for effective capture of CO₂, *AIChE J.* 64 (2018) 632–639, <https://doi.org/10.1002/aic.15952>.
- Y.-M. Liu, Z. Tian, F. Qu, Y. Zhou, Y. Liu, D.-J. Tao, Tuning ion-pair interaction in cuprous-based protic ionic liquids for significantly improved CO capture ACS, *Sustainable Chem. Eng.* 7 (2019) 11894–11900, <https://doi.org/10.1021/acssuschemeng.9b02540>.
- M. Ghafari, J.D. Atkinson, One-step hyper-cross-linking of porous styrenic polymers using dichloroalkane cross-linkers to maintain hydrophobicity, *Polymer* 116 (2017) 278–286, <https://doi.org/10.1016/j.polymer.2017.03.082>.
- Z. Fu, J. Jia, J. Li, C. Liu, Transforming waste expanded polystyrene foam into hyper-crosslinked polymers for carbon dioxide capture and separation, *Chem. Eng. J.* 323 (2017) 557–564, <https://doi.org/10.1016/j.cej.2017.04.090>.
- G. Ren, Q. Chen, J. Zheng, B. Huang, Y. Qian, N-doped carbon nanofibers aerogels derived from aramid as efficient electrocatalysts for oxygen reduction reaction in alkaline and acidic media, *J. Electroanal. Chem.* 829 177 (2018) 183, <https://doi.org/10.1016/j.jelechem.2018.09.050>.
- Y. Yang, Q. Zhang, S. Zhang, S. Li, Synthesis and characterization of triphenylamine-containing microporous organic copolymers for carbon dioxide uptake, *Polymer* 54 5698 (5702) (2013), <https://doi.org/10.1016/j.polymer.2013.08.039>.
- X. Zhao, Y. Zhou, K. Huang, C. Li, D.-J. Tao, Ultralow loading cobalt-based nanocatalyst for benign and efficient aerobic oxidation of allylic alcohols and biobased olefins, *ACS Sustainable Chem. Eng.* 7 (2018) 1901–1908, <https://doi.org/10.1021/acssuschemeng.8b03678>.
- F. Liu, K. Huang, Q. Wu, S. Dai, Solvent-free self-assembly to the synthesis of nitrogen-doped ordered mesoporous polymers for highly selective capture and conversion of CO₂ *Adv. Mater.* 29 (2017), <https://doi.org/10.1002/adma.201700445>.
- A. Wang, R. Fan, X. Pi, Y. Zhou, G. Chen, W. Chen, Y. Yang, Nitrogen-doped microporous carbons derived from pyridine ligand-based metal-organic complexes as high-performance SO₂ adsorption sorbents, *ACS Appl. Mater. Interfaces* 10 (2018) 37407–37416, <https://doi.org/10.1021/acsami.8b12739>.
- Y. Zhang P. Zhang W. Yu J. Zhang J. Huang J. Wang M. Xu Q. Deng Z. Zeng S. Deng Highly selective and reversible sulfur dioxide adsorption on a microporous metal-organic framework via polar sites *ACS Appl. Mater. Interfaces* 11 2019 10680 10688 10.1021/acsami.9b01423.
- N. Karatepe, İ. Orbak, R. Yavuz, A. Özyüğüran, Sulfur dioxide adsorption by activated carbons having different textural and chemical properties, *Fuel* 87 3207 (3215) (2008), <https://doi.org/10.1016/j.fuel.2008.06.002>.
- L. Yue, L. Rao, L. Wang, L. An, C. Hou, C. Ma, H. DaCosta, X. Hu, Efficient CO₂ adsorption on nitrogen-doped porous carbons derived from d-glucose, *Energy & Fuels* 32 6955 (6963) (2018), <https://doi.org/10.1021/acs.energyfuels.8b01028>.
- S.I. Garcés-Polo, J. Villarroya-Rocha, K. Sapag, S.A. Korili, A. Gil, A comparative study of CO₂ diffusion from adsorption kinetic measurements on microporous materials at low pressures and temperatures, *Chem. Eng. J.* 302 (2016) 278–286, <https://doi.org/10.1016/j.cej.2016.05.057>.

- [41] C. Wang, G. Cui, X. Luo, Y. Xu, H. Li, S. Dai, Highly efficient and reversible SO₂ capture by tunable azole-based ionic liquids through multiple-site chemical absorption, *J. Am. Chem. Soc.* 133 (2011) 11916–11919, <https://doi.org/10.1021/ja204808h>.
- [42] K. Tan, P. Canepa, Q. Gong, J. Liu, D.H. Johnson, A. Dyevoich, P.K. Thallapally, T. Thonhauser, J. Li, Y.J. Chabal, Mechanism of preferential adsorption of SO₂ into two microporous paddle wheel frameworks M(bdc)(ted)0.5, *Chem. Mater.* 25 4653 (4662) (2013), <https://doi.org/10.1021/cm401270b>.
- [43] G. Cui, W. Lin, F. Ding, X. Luo, X. He, H. Li, C. Wang, Highly efficient SO₂ capture by phenyl-containing azole-based ionic liquids through multiple-site interactions, *Green Chem.* 16 (2014) 1211–1216, <https://doi.org/10.1039/C3GC41458B>.